Multiscale solutions of radiative heat transfer by the discrete unified gas kinetic scheme

Xiao-Ping Luo, Cun-Hai Wang, Yong Zhang, Hong-Liang Yi,* and He-Ping Tan

Key Laboratory of Aerospace Thermophysics, Ministry of Industry and Information Technology, School of Energy Science and Engineering, Harbin Institute of Technology, 92 West Dazhi Street, Harbin 150001, China

(Received 31 January 2018; published 7 June 2018)

The radiative transfer equation (RTE) has two asymptotic regimes characterized by the optical thickness, namely, optically thin and optically thick regimes. In the optically thin regime, a ballistic or kinetic transport is dominant. In the optically thick regime, energy transport is totally dominated by multiple collisions between photons; that is, the photons propagate by means of diffusion. To obtain convergent solutions to the RTE, conventional numerical schemes have a strong dependence on the number of spatial grids, which leads to a serious computational inefficiency in the regime where the diffusion is predominant. In this work, a discrete unified gas kinetic scheme (DUGKS) is developed to predict radiative heat transfer in participating media. Numerical performances of the DUGKS are compared in detail with conventional methods through three cases including one-dimensional transient radiative heat transfer, two-dimensional steady radiative heat transfer, and three-dimensional multiscale radiative heat transfer. Due to the asymptotic preserving property, the present method with relatively coarse grids gives accurate and reliable numerical solutions for large, small, and in-between values of optical thickness, and, especially in the optically thick regime, the DUGKS demonstrates a pronounced computational efficiency advantage over the conventional numerical models. In addition, the DUGKS has a promising potential in the study of multiscale radiative heat transfer inside the participating medium with a transition from optically thin to optically thick regimes.

DOI: 10.1103/PhysRevE.97.063302

I. INTRODUCTION

Photon transport, conventionally called radiation transport, plays an important role in laser materials processing [1], optical tomography [2], solar energy harvesting [3], combustion systems [4], and many other applications [5,6]. Hence large scientific efforts have been invested to tackle a wide range of radiative heat transfer problems in the past 50 years. Since exact analytical solutions are available only in a few simplified cases, a full understanding of radiative transport phenomena in more complicated cases (i.e., nonhomogeneous, nonisothermal, scattering, nongray media, and collimated intensities) requires the numerical solution to the radiative transfer equation (RTE). The RTE is an integrodifferential equation in terms of radiative intensity which is a function in seven-dimensional phase space. Due to the high dimensionality of RTE, the presence of integral coupling terms, and the complexity of the radiative transfer problem, finding its numerical solution is a challenging task. Efficient, accurate, and stable simulation techniques are in urgent need for the analysis of radiative transfer in participating media.

Over the years, various numerical methods based on the RTE have been developed and implemented, including the zonal method [7], the spherical harmonics method [8], the discrete transfer method (DTM) [9,10], the discrete ordinates method (DOM) [11], the finite volume method (FVM) [12], the finite element method (FEM) [13–15], the meshless method [16–18], and Monte Carlo method (MCM) [19,20]. Detailed reviews of the different methods are available in the literature [21,22]. Among these methods, DOM, FVM, and FEM are deterministic schemes and solve the RTE by angular and space discretization. These deterministic methods have achieved great success in dealing with radiative transport in relatively optically thin media (the optical thickness or the reciprocal of Knudsen number is often less than 6). For photon transport in thick media where temporal and spatial scales of different magnitudes come into play, the treatment of a small mean free path (MFP) poses great computational challenge. From a numerical point of view, the numerical stability for explicit schemes requires a mesh size smaller than the MFP of photons and a time step with the order of the square of the mean free path in transient calculations due to the usual parabolic Courant-Friedrichs-Lewy (CFL) condition [23]. An implicit scheme has no such restriction on the time step, but a large algebraic system involving the information of the total grid system needs to invert. These constraints make the numerical solution of the RTE computationally expensive for the optically thick medium. On the other hand, as a probabilistic approach, MCM is to trace the physical process of radiative transfer by random simulation of photon bundle behaviors happening in participating media. So no angular discretization is required and the MCM solutions are often considered the benchmark. Despite the great success in the simulation of radiative transfer by MCM, MCM becomes very costly in the diffusive regime (the optical thickness of the medium is high) due to frequent collision of photons. What is worse is that the statistical certainty of MCM may generate noisy results. A well-known way to tackle the radiative transport problem in thick media is based on the diffusive equation (DE) where the P1 approximation

*Corresponding author: yihongliang@hit.edu.cn

and diffusion approximations are assumed, which is easier and faster. However, the DE-based method is not accurate in a lot of physical simulations and fails to describe both short-time and long-time radiation transport when the medium is not optically thick. In fact, the radiative transfer exhibits multiscale characteristics with the change of optical thickness. In the medium with a small optical thickness, a ballistic or kinetic transport dominates, while as the optical thickness increases, the collision between photons becomes frequent, and a diffusive transport characteristic gradually appears; that is, in the situation the thermal radiation is transferred by means of diffusion. In summary, it is necessary to develop multiscale schemes which can efficiently and accurately solve radiative transfer not only in optically thin media but also in optically thick media.

The first kind of multiscale technique is to couple the RTE model and DE model in a domain-decomposition framework. However, the coupling condition of different models is often difficult to obtain. To settle the coupling problem, Roger and Crouseilles introduced a smooth transition region called a buffer zone which matches the RTE model and DE model [23]. The second possibility is given by using the micro-macro model [24,25] or its variant, the hybrid transport-diffusion (HTD) model, proposed by Roger *et al.* [26]. In the micro-macro model, the radiation intensity is decomposed into two parts, a mesoscopic component and a macroscopic component, and the component equations are established accordingly. However, the coupling treatment of equations for the two components is a tough problem. The HTD model decouples the two equations and thus the artificial boundary condition for the macroscopic component is avoided. The macroscopic equation in this model is solved independently without the coupling with the mesoscopic equation. As a result, The HTD model shows a significant improvement in the numerical implementation in comparison with the standard micro-macro formulation. The third possible approach for such multiscale radiation problems is the asymptotic preserving (AP) method. Comparing with domain-decomposition or intensity-decomposition-type methods, the AP methods avoid the coupling of different models. The AP methods solve the RTE in the entire domain and make a fully consistent discretization of the DE model automatically in the optically thick limit with a fixed computational grid. The AP methods capture the radiation diffusion limit efficiently in the optically thick regime without numerically resolving the small MFP of photons. So the AP methods have great potential to provide accurate results for radiative transfer with small computational cost for various optical thicknesses.

One of the AP methods that has been successful in doing that is the so-called unified gas kinetic scheme (UGKS) [27,28]. By utilizing the coupling treatment of photon transport and collision in the flux construction, the UGKS can accurately and efficiently capture numerical solutions to both the linear radiation transport equation [27] and the nonlinear radiation transport equation [28] without using a mesh size smaller than the photon MFP. For the attractive property and great potential applications, the UKGS is subsequently extended to frequency-dependent radiative systems [29]. In a recent study, an implicit UGKS was developed for both gray and frequency-dependent radiative systems with strong isotropic scattering [30]. With an implicit formulation, the CFL constraint on the numerical time step is much relaxed and a large time step is used in simulations, resulting in a considerable improvement in computational efficiency. Later, the implicit UGKS was further extended to a multidimensional radiative system with complex geometry by using the unstructured mesh technique [31].

In this series of work, we aim to develop another asymptotic-preserving method, the so-called discrete unified gas kinetic scheme (DUGKS), for radiative transfer problems. The DUGKS is a simplification of UGKS and was designed originally for solving the Boltzmann equation by Guo *et al.* [32,33]. Similar to UGKS, the DUGKS is a hybrid of the discrete velocity method (for velocity space, or the discrete ordinate method for angle space) and the finite volume method with special spatial discretization schemes. Both DUGKS and UGKS have an asymptotic-preserving property. However, they differ completely in the flux construction. In the DUGKS, the flux construction is simplified and the numerical flux at a cell interface is evaluated by integrating the kinetic equation along the characteristic line while the numerical flux in the UGKS is approximated by the local integral solution of the kinetic equation [34]. On the other hand, through employing variable transformation, the evolution of macroscopic variables in UGKS is not required in DUGKS. In some sense, the DUGKS can also be considered a finite volume version of the lattice Boltzmann method (LBM) and it takes advantage of the geometrical flexibility and strong conservation property of the FVM. Like the LBM, DUGKS is also explicit and can be easily adapted for parallel computing. In addition, easy boundary treatments, the bounce-back rule, and the nonequilibrium extrapolation scheme widely used in LBM are also employed in the DUGKS framework. However, quite different from other versions of off-lattice Boltzmann method, DUGKS has an asymptotic-preserving property, has low numerical dissipation, and satisfies numerical stability even at a big time step size. This approach removes the tight bound on the maximally allowed time step via applying a semi-implicit treatment of the collision term and evaluating the cell interface flux of the convective term at a temporal midpoint. In other words, the tie-up of mesh spacing and time step that exists in the conventional LBM and other explicit schemes is completely removed. Of late, as one of the efficient and robust multiscale methods, DUGKS has been already applied to a wide range of problems including nonequilibrium gas flow [35], natural convection [36], and phonon conduction [37,38]. Due to the similarity of the intrinsic kinetic nature of molecules, phonons, and photons, it is natural to solve the RTE by DUGKS. Indeed, The RTE can be considered a linear variant of the Boltzmann equation. The present study is aimed at demonstrating the applicability of this method to various problems encountered in radiative heat transfer.

The remainder of this paper is organized as follows. Section II gives a short overview of RTE. Section III generalizes the idea of DUGKS for solving RTE and gives the implementation details. Several numerical cases are addressed in Sec. IV. Finally, we make a conclusion in Sec. V with a brief summary.

II. KINETIC THEORY OF PHOTONS AND RADIATIVE TRANSFER EQUATION

The Boltzmann equation for photon gases accounts for photon distribution changes in the phase space number density as the photons stream along their geodesics. In the absence of general relativistic effects, the most known Boltzmann equation can be written mathematically as

$$\frac{\partial f(\mathbf{x},\mathbf{s},v,t)}{\partial t} + c\mathbf{s}\cdot\nabla f(\mathbf{x},\mathbf{s},v,t) = Q[f(\mathbf{x},\mathbf{s},v,t)], \quad (1)$$

where f is the number density distribution function of photons in terms of the seven independent variables $(\mathbf{x},\mathbf{s},\nu,t)$ and c is the speed of photons; $\mathbf{x}$ is a spatial position vector, $\mathbf{s}$ is the direction vector of photon propagation, ν is the photon frequency, and t is a temporal variable. The second term on the left-hand side of Eq. (1) is the convective term, representing the difference between the numbers of photons entering and leaving the region per unit volume. On the right-hand side of Eq. (1), Q is the collision operator, accounting for the interactions between photons and surrounding matter. Since the heat transfer is of concern, another fundamental quantity, the specific intensity of photons, is defined as $I = h\nu cf$ with the Planck constant h. The specific intensity stands for the energy carried by photons per unit area, time, frequency interval, and solid angle, crossing a small test surface which is oriented normal to the propagation direction of phonons. The specific intensity provides a complete mesoscopic description of the unpolarized radiation field. Ignoring the frequency dependence, Eq. (1) can be rewritten in terms of the radiative intensity:

$$\frac{1}{c}\frac{\partial I(\mathbf{x},\mathbf{s},t)}{\partial t} + \mathbf{s}\cdot\nabla I(\mathbf{x},\mathbf{s},t) = h\nu Q[I(\mathbf{x},\mathbf{s},t)]. \quad (2)$$

From the point of view of phenomenology, the interactions of attenuation and augmentation by absorption, emission, and scattering processes are commonly taken into account [39,40]. Hence the collision integral term on the right-hand side of Eq. (2) can be expressed as follows:

$$h\nu Q[I(\mathbf{x},\mathbf{s},t)] = -\beta I(\mathbf{x},\mathbf{s},t) + \beta(1-\omega)I_{\mathrm{b}}(\mathbf{x},t) + \frac{\beta\omega}{4\pi}\int_{4\pi} I\left(\mathbf{x},\mathbf{s}',t\right)\Phi(\mathbf{s}',\mathbf{s})\mathrm{d}\Omega', \quad (3)$$

where I_{b} is the blackbody intensity, Φ is the scattering phase function, $\beta = \beta(\mathbf{x})$ is the extinction coefficient which is related to the local MFP of photon gas, and $\omega = \omega(\mathbf{x})$ is the scattering albedo. Substituting Eq. (3) into Eq. (2), we obtain the radiative transfer equation,

$$\frac{1}{c}\frac{\partial I(\mathbf{x},\mathbf{s},t)}{\partial t} + \mathbf{s}\cdot\nabla I(\mathbf{x},\mathbf{s},t) = -\beta I(\mathbf{x},\mathbf{s},t) + \beta(1-\omega)I_{\mathrm{b}}(\mathbf{x},t) + \frac{\beta\omega}{4\pi}\int_{4\pi} I(\mathbf{x},\mathbf{s}',t)\Phi(\mathbf{s}',\mathbf{s})\mathrm{d}\Omega', \quad (4)$$

which describes the radiative transport in an absorbing, emitting, and scattering medium under local thermal equilibrium. In the present work, diffusely emitting and reflecting boundaries are considered, and the general boundary condition for Eq. (4) is

$$I(\mathbf{x}_{\mathrm{w}},\mathbf{s},t) = (1-\rho_{\mathrm{w}})I^{\mathrm{ext}}(\mathbf{x}_{\mathrm{w}},\mathbf{s},t) + \varepsilon_{\mathrm{w}}I_{\mathrm{b}}(\mathbf{x}_{\mathrm{w}}) + \frac{\rho_{\mathrm{w}}}{\pi}\int_{\mathbf{n}_{\mathrm{w}}\cdot\mathbf{s}'<0}(\mathbf{n}_{\mathrm{w}}\cdot\mathbf{s}')I(\mathbf{x}_{\mathrm{w}},\mathbf{s}',t)\mathrm{d}\Omega', \quad (5)$$

where $I^{\mathrm{ext}}(\mathbf{x}_{\mathrm{w}},\mathbf{s},t)$ is the externally incident radiation, ε_{w} is the diffuse emissivity, ρ_{w} is the diffuse reflectivity, and $\mathbf{n}_{\mathrm{w}}$ is the unit inner normal vector at the boundary. $I_{\mathrm{b}}(\mathbf{x}_{\mathrm{w}})$ is the blackbody radiation intensity at the boundary surface having a specified temperature. It should be noted that for opaque boundaries, the first term on the right-hand side is omitted, and for semitransparent ones, the second term is not considered. In order to reduce the ray effect caused by discontinuities or abrupt changes of the wall temperature, some modifications are made. Following Refs. [41,42], we decompose the radiation intensity into two parts: a direct intensity component $I_{\mathrm{c}}(\mathbf{x},\mathbf{s},t)$ due to externally incident collimated radiation after partial extinction, by absorption and scattering, along its paths, and a diffuse intensity component $I_{\mathrm{d}}(\mathbf{x},\mathbf{s},t)$, resulting from emission from the boundaries, emission from within the medium, and the radiation scattered away from the collimated irradiation, that is, $I(\mathbf{x},\mathbf{s},t) = I_{\mathrm{c}}(\mathbf{x},\mathbf{s},t) + I_{\mathrm{d}}(\mathbf{x},\mathbf{s},t)$.

$$\frac{1}{c}\frac{\partial I_{\mathrm{c}}(\mathbf{x},\mathbf{s},t)}{\partial t} + \mathbf{s}\cdot\nabla I_{\mathrm{c}}(\mathbf{x},\mathbf{s},t) = -\beta I_{\mathrm{c}}(\mathbf{x},\mathbf{s},t), \quad (6)$$

$$\frac{1}{c}\frac{\partial I_{\mathrm{d}}(\mathbf{x},\mathbf{s},t)}{\partial t} + \mathbf{s}\cdot\nabla I_{\mathrm{d}}(\mathbf{x},\mathbf{s},t) = -\beta I_{\mathrm{d}}(\mathbf{x},\mathbf{s},t) + \beta(1-\omega)I_{\mathrm{b}}(\mathbf{x},t) + \frac{\beta\omega}{4\pi}\int_{4\pi} I(\mathbf{x},\mathbf{s}',t)\Phi(\mathbf{s}',\mathbf{s})\mathrm{d}\Omega', \quad (7)$$

subject to the boundary conditions

$$I_{\mathrm{c}}(\mathbf{x}_{\mathrm{w}},\mathbf{s},t) = (1-\rho_{\mathrm{w}})I^{\mathrm{ext}}(\mathbf{x}_{\mathrm{w}},\mathbf{s},t), \quad (8)$$

$$I_{\mathrm{d}}(\mathbf{x}_{\mathrm{w}},\mathbf{s},t) = \varepsilon_{\mathrm{w}}I_{\mathrm{b}}(\mathbf{x}_{\mathrm{w}},t) + \frac{\rho_{\mathrm{w}}}{\pi}\int_{\mathbf{n}_{\mathrm{w}}\cdot\mathbf{s}'<0}(\mathbf{n}_{\mathrm{w}}\cdot\mathbf{s}')I(\mathbf{x}_{\mathrm{w}},\mathbf{s}',t)\mathrm{d}\Omega'. \quad (9)$$

With the boundary conditions, the solution to Eq. (6) can be given analytically as [26]

$$I_{\mathrm{c}}(\mathbf{x},\mathbf{s},t) = (1-\rho_{\mathrm{w}})I^{\mathrm{ext}}\left(\mathbf{x}_{\mathrm{w}},\mathbf{s},t-\frac{\|\mathbf{x}-\mathbf{x}_{\mathrm{w}}\|}{c}\right) \times \exp\left(-\int_0^{\|\mathbf{x}-\mathbf{x}_{\mathrm{w}}\|}\beta\mathrm{d}l\right). \quad (10)$$

After that, Eq. (7) can be solved numerically, which is illustrated in the following section.

III. DISCRETE UNIFIED GAS KINETIC SCHEME FOR RTE

In this section, we extend the spirit of DUGKS in Refs. [32,33] to the gray radiative transfer system. For simplicity, only isotropic scattering ($\Phi = 1$) is considered in this work. Similar to other deterministic approaches, the DUGKS solves the RTE by the discretization of angle space and physical space. The starting point is the angular discretization. The

DOM is employed for the angular variable of Eq. (7). The integration over a solid angle is evaluated by a quadrature over a representative finite set of directions according to a certain quadrature rule (e.g., Gauss-Legendre quadrature, Gauss-Chebyshev quadrature, S_N quadrature, etc.). Thus the corresponding discrete ordinate form of Eq. (7) can be written as

$$\frac{1}{c}\frac{\partial I_{\rm d}(\mathbf{x},\mathbf{s}_k,t)}{\partial t}+\mathbf{s}_k\cdot\nabla I_{\rm d}(\mathbf{x},\mathbf{s}_k,t)=-\beta I_{\rm d}(\mathbf{x},\mathbf{s}_k,t)+\beta(1-\omega)I_{\rm b}(\mathbf{x},t)+\frac{\beta\omega}{4\pi}\sum_m I(\mathbf{x},\mathbf{s}_m,t)w_m, \tag{11}$$

where w_m is the weight assigned to the direction $\mathbf{s}_m$. The sum of the weights is equal to the area of the surface of a unit sphere. Spatial discretization and time integration are treated separately. For time variables, let $t_{\rm n}=n\,\Delta t$, where Δt is the time step. The physical space is discretized into a set of cells and the terms on both sides of Eq. (11) are integrated over every cell as done in the finite volume method. $I_{\rm d}\ (\mathbf{x}_j,\mathbf{s}_k,t_k)$ denote the cell averaged value for the diffuse intensity at time t_n in cell j with control volume of V_j located at $\mathbf{x}_j$ along photon propagation direction $\mathbf{s}_k$. Following Refs. [32,33], integrating Eq. (11) over cell j and applying the trapezoidal rule for the collision term, conventionally called the radiative source term in radiative transfer theory, yields that

$$\begin{aligned}&\frac{I_{\rm d}(\mathbf{x}_j,\mathbf{s}_k,t_{n+1})-I_{\rm d}(\mathbf{x}_j,\mathbf{s}_k,t_n)}{c}+\frac{1}{V_j}\int_{t_n}^{t_{n+1}}\int_{V_j}\mathbf{s}_k\cdot\nabla I_{\rm d}(\mathbf{x},\mathbf{s}_k,t)\mathrm{d}V\,\mathrm{d}t\\&=\frac{\beta\Delta t}{2}\left[(1-\omega)I_{\rm b}(\mathbf{x}_j,t_{n+1})+\frac{\omega}{4\pi}\sum_m I(\mathbf{x}_j,\mathbf{s}_m,t_{n+1})w_m-I_{\rm d}(\mathbf{x}_j,\mathbf{s}_k,t_{n+1})\right]\\&\quad+\frac{\beta\Delta t}{2}\left[(1-\omega)I_{\rm b}(\mathbf{x}_j,t_n)+\frac{\omega}{4\pi}\sum_m I(\mathbf{x}_j,\mathbf{s}_m,t_n)w_m-I_{\rm d}(\mathbf{x}_j,\mathbf{s}_k,t_n)\right].\end{aligned} \tag{12}$$

Rearranging for the evolution equation in time and introducing the two variables

$$\tilde{I}(\mathbf{x},\mathbf{s},t)=I_{\rm d}(\mathbf{x},\mathbf{s},t)+\frac{\chi}{2}\left[I_{\rm d}(\mathbf{x},\mathbf{s},t)-(1-\omega)I_{\rm b}(\mathbf{x},t)-\frac{\omega}{4\pi}\int_{4\pi}I(\mathbf{x},\mathbf{s}',t)\mathrm{d}\Omega'\right], \tag{13}$$

$$\tilde{I}^{+}(\mathbf{x},\mathbf{s},t)=I_{\rm d}(\mathbf{x},\mathbf{s},t)-\frac{\chi}{2}\left[I_{\rm d}(\mathbf{x},\mathbf{s},t)-(1-\omega)I_{\rm b}(\mathbf{x},t)-\frac{\omega}{4\pi}\int_{4\pi}I(\mathbf{x},\mathbf{s}',t)\mathrm{d}\Omega'\right], \tag{14}$$

with $\chi=\mathrm{c}\Delta t\beta$, Eq. (12) may be rendered into a fully explicit form:

$$\tilde{I}(\mathbf{x}_j,\mathbf{s}_k,t_{n+1})=\tilde{I}^{+}(\mathbf{x}_j,\mathbf{s}_k,t_n)-\frac{c}{V_j}\int_{t_n}^{t_{n+1}}\int_{V_j}\mathbf{s}_k\cdot\nabla I_{\rm d}(\mathbf{x},\mathbf{s}_k,t)\mathrm{d}V\,\mathrm{d}t. \tag{15}$$

By applying the Gauss divergence theorem and midpoint rule for the time integration, the convective term can be approximated by

$$\frac{c}{V_j}\int_{t_n}^{t_{n+1}}\int_{V_j}\mathbf{s}_k\cdot\nabla I_{\rm d}(\mathbf{x},\mathbf{s}_k,t)\mathrm{d}V\,\mathrm{d}t=\frac{c\Delta t}{V_j}\sum_f(\mathbf{s}_k\cdot\mathbf{n}_f)I_{\rm d}(\mathbf{x}_f,\mathbf{s}_k,t_{n+1/2})\Delta S_f, \tag{16}$$

where $\mathbf{n}_f$ and ΔS_f are the outer normal vector and control area of the interface, respectively. $I_{\rm d}\ (\mathbf{x}_f,\mathbf{s}_k,t_{n+1/2})$ denotes the mean radiative intensity at time $t_{n+1/2}=(2n+1)\Delta t/2$ at the cell interface along photon transport direction $\mathbf{s}_k$. The numerical flux over the boundary of the cell is approximated by the summation over the cell interfaces of the integrand function. The subscript f denotes a cell interface under consideration. In order to update the system (15), we have to determine all terms unknown in Eq. (15). First, we integrate Eq. (11) along the characteristic line within a half time step and also approximate the right-hand term of Eq. (11) by the trapezoidal rule. This yields the following discrete equation:

$$\begin{aligned}&\frac{I_{\rm d}(\mathbf{x}_f,\mathbf{s}_k,t_{n+1/2})-I_{\rm d}(\mathbf{x}_f-\mathbf{s}_k ch,\mathbf{s}_k,t_n)}{c}\\&=\frac{\beta h}{2}\left[(1-\omega)I_{\rm b}(\mathbf{x}_f,t_{n+1/2})+\frac{\omega}{4\pi}\sum_m I(\mathbf{x}_f,\mathbf{s}_m,t_{n+1/2})w_m-I_{\rm d}(\mathbf{x}_f,\mathbf{s}_k,t_{n+1/2})\right]\\&\quad+\frac{\beta h}{2}\left[(1-\omega)I_{\rm b}(\mathbf{x}_f-\mathbf{s}_k ch,t_n)+\frac{\omega}{4\pi}\sum_m I(\mathbf{x}_f-\mathbf{s}_k ch,\mathbf{s}_m,t_n)w_m-I_{\rm d}(\mathbf{x}_f-\mathbf{s}_k ch,\mathbf{s}_k,t_n)\right]\end{aligned} \tag{17}$$

with $h=\Delta t/2$. In order to remove the implicity, another two new variables are introduced:

$$\bar{I}(\mathbf{x},\mathbf{s},t)=I_{\rm d}(\mathbf{x},\mathbf{s},t)+\frac{\chi}{4}\left[I_{\rm d}(\mathbf{x},\mathbf{s},t)-(1-\omega)I_{\rm b}(\mathbf{x},t)-\frac{\omega}{4\pi}\int_{4\pi}I(\mathbf{x},\mathbf{s}',t)\mathrm{d}\Omega'\right], \tag{18}$$

$$\bar{I}^{+}(\mathbf{x},\mathbf{s},t) = I_{\mathrm{d}}(\mathbf{x},\mathbf{s},t) - \frac{\chi}{4}\left[I_{\mathrm{d}}(\mathbf{x},\mathbf{s},t) - (1-\omega)I_{\mathrm{b}}(\mathbf{x},t) - \frac{\omega}{4\pi}\int_{4\pi} I(\mathbf{x},\mathbf{s}',t)\mathrm{d}\Omega'\right]. \tag{19}$$

Substituting the above two equations into Eq. (17), we can obtain

$$\bar{I}(\mathbf{x}_f,\mathbf{s}_k,t_{n+1/2}) = \bar{I}^{+}(\mathbf{x}_f - \mathbf{s}_k ch,\mathbf{s}_k,t_n). \tag{20}$$

Since the position $\mathbf{x}_f - \mathbf{s}_k ch$ may not be located at the cell center, the unknown variable $\bar{I}^{+}(\mathbf{x}_f - \mathbf{s}_k ch,\mathbf{s}_k,t_n)$ in Eq. (20) can be approximated by linear interpolation (other high-order interpolations are also available), as done in Refs. [33,37]. To avoid the creation of artificial oscillations in the solution, the van Leer limiter is used in the gradient reconstruction. Then the diffuse component $I_{\mathrm{d}}(\mathbf{x},\mathbf{s},t)$ can be computed as

$$\begin{aligned} I_{\mathrm{d}}(\mathbf{x},\mathbf{s},t) = {} & \frac{4}{4+\chi}\bar{I}(\mathbf{x},\mathbf{s},t) + \frac{4\chi\omega}{\pi(4+\chi)[4+\chi(1-\omega)]}\int_{4\pi}\bar{I}(\mathbf{x},\mathbf{s}',t)\mathrm{d}\Omega' \\ & + \frac{\chi(1-\omega)}{4+\chi(1-\omega)}I_{\mathrm{b}}(\mathbf{x},t) + \frac{\chi\omega}{\pi[4+\chi(1-\omega)]}\int_{4\pi} I_{\mathrm{c}}(\mathbf{x},\mathbf{s}',t)\mathrm{d}\Omega'. \end{aligned} \tag{21}$$

Combining Eqs. (13), (14), and (19), we also obtain

$$\tilde{I}^{+}(\mathbf{x},\mathbf{s},t) = \frac{4}{3}\bar{I}^{+}(\mathbf{x},\mathbf{s},t) - \frac{1}{3}\tilde{I}(\mathbf{x},\mathbf{s},t), \tag{22}$$

$$\begin{aligned} \bar{I}^{+}(\mathbf{x},\mathbf{s},t) = {} & \frac{4-\chi}{4+2\chi}\tilde{I}(\mathbf{x},\mathbf{s},t) + \frac{3\chi\omega}{[2+\chi(1-\omega)](2+\chi)}\frac{1}{4\pi}\int_{4\pi}\tilde{I}(\mathbf{x},\mathbf{s}',t)\mathrm{d}\Omega' + \frac{3\chi(1-\omega)}{4+2\chi(1-\omega)}I_{\mathrm{b}}(\mathbf{x},t) \\ & + \frac{3\chi\omega}{4+2\chi(1-\omega)}\frac{1}{4\pi}\int_{4\pi} I_{\mathrm{c}}(\mathbf{x},\mathbf{s}',t)\mathrm{d}\Omega'. \end{aligned} \tag{23}$$

In Eqs. (21) and (23), the black radiative intensity $I_{\mathrm{b}}(\mathbf{x},t)$ is still unknown and will be computed next. At radiative equilibrium, the blackbody intensity is calculated by considering the energy conservation condition, that is,

$$\begin{aligned} I_{\mathrm{b}}(\mathbf{x},t) &= \frac{1}{4\pi}\int_{4\pi} I(\mathbf{x},\mathbf{s},t)\mathrm{d}\Omega \\ &= \frac{1}{4\pi}\int_{4\pi}\tilde{I}(\mathbf{x},\mathbf{s},t)\mathrm{d}\Omega + \left(1+\frac{\chi}{2}\right)\frac{1}{4\pi}\int_{4\pi} I_{\mathrm{c}}(\mathbf{x},\mathbf{s},t)\mathrm{d}\Omega \\ &= \frac{1}{4\pi}\int_{4\pi}\bar{I}(\mathbf{x},\mathbf{s},t)\mathrm{d}\Omega + \left(1+\frac{\chi}{4}\right)\frac{1}{4\pi}\int_{4\pi} I_{\mathrm{c}}(\mathbf{x},\mathbf{s},t)\mathrm{d}\Omega. \end{aligned} \tag{24}$$

The radiative equilibrium condition implies that the volumetric absorption equals the volumetric emission. For simple radiative nonequilibrium problems, the temperature field of the medium or the emission power field is commonly given. In the former case, the blackbody intensity is calculated by the Stefan-Boltzmann law,

$$I_{\mathrm{b}}(\mathbf{x},t) = \sigma T^4(\mathbf{x},t), \tag{25}$$

in which σ is the Stefan-Boltzmann constant and T is the local temperature of the medium under local thermal equilibrium.

Up to now, only time step left is unknown. Note that the treatment of both convective and collision terms is semi-implicit in the DUGKS framework. The present method is stable without resolving the scales of photon MFP. The principle for the choice of Δt is that the free transport distance in a cell, $c\Delta t$, should be smaller than the cell size to avoid extrapolation, i.e., $c\Delta t < \Delta x$ with Δx the minimal grid spacing. This condition can also be written as a form of the CFL condition,

$$\Delta t = \alpha\frac{\Delta x}{c}, \tag{26}$$

where $0 < \alpha < 1$ is the CFL number. It is obvious that the maximum stable time step is not limited by the extinction coefficient.

For the black wall, a photon is absorbed as it hits the wall, and a new photon in thermal equilibrium with boundary temperature is emitted into the domain. For the gray wall, some of the incident photons are absorbed and the rest are reflected diffusively back to the domain, depending on the reflectivity of the wall. The general boundary condition can be expressed mathematically as

$$\begin{aligned} I_{\mathrm{d}}(\mathbf{x}_{\mathrm{w}},\mathbf{s}_k,t_n) = {} & \varepsilon_{\mathrm{w}} I_{\mathrm{b}}(\mathbf{x}_{\mathrm{w}}) + \frac{\rho_{\mathrm{w}}}{\pi}\sum_{\mathbf{n}_{\mathrm{w}}\cdot\mathbf{s}'_m<0}(\mathbf{n}_{\mathrm{w}}\cdot\mathbf{s}'_m) \\ & \times I(\mathbf{x}_{\mathrm{w}},\mathbf{s}'_m,t_n)w_m,\mathbf{n}_{\mathrm{w}}\cdot\mathbf{s}_k > 0, \end{aligned} \tag{27}$$

where $\mathbf{s}_k$ and $\mathbf{s}'_m$ are the directions of propagation and incidence, respectively.

In practical simulations, the direct intensity component is calculated analytically. The transformed intensities $\tilde{I}(\mathbf{x},\mathbf{s},t)$ and $\bar{I}^{+}(\mathbf{x},\mathbf{s},t)$ are stored and updated with time. In summary, the DUGKS algorithm employed to solve the RTE can thus be listed as follows:

$$\begin{aligned} & I_{\mathrm{c}}(\mathbf{x}_j,\mathbf{s}_k,t_n) \text{ and } \tilde{I}(\mathbf{x}_j,\mathbf{s}_k,t_n) \\ & \xrightarrow{(22),(23)} \bar{I}^{+}(\mathbf{x}_j,\mathbf{s}_k,t_n) \text{ and } \tilde{I}^{+}(\mathbf{x}_j,\mathbf{s}_k,t_n) \\ & \xrightarrow{(20)} \bar{I}(\mathbf{x}_f,\mathbf{s}_k,t_{n+1/2}) \\ & \xrightarrow{(21)} I_{\mathrm{d}}(\mathbf{x}_f,\mathbf{s}_k,t_{n+1/2}) \\ & \xrightarrow{(15)} \tilde{I}(\mathbf{x}_j,\mathbf{s}_k,t_{n+1}). \end{aligned}$$

Once the transformed intensity distribution is known, the local incident radiation and net radiative flux can be also obtained by

$$G = \int_{4\pi} I(\mathbf{x},\mathbf{s},t)\mathrm{d}\Omega = \frac{2}{2+\chi(1-\omega)}\int_{4\pi}\tilde{I}(\mathbf{x},\mathbf{s},t)\mathrm{d}\Omega + \frac{\chi(1-\omega)}{2+\chi(1-\omega)}4\pi I_{\mathrm{b}}(\mathbf{x},t) + \frac{2+\chi}{2+\chi(1-\omega)}\int_{4\pi} I_{\mathrm{c}}(\mathbf{x},\mathbf{s},t)\mathrm{d}\Omega, \quad (28)$$

$$\mathbf{q} = \int_{4\pi} I(\mathbf{x},\mathbf{s},t)\mathbf{s}\mathrm{d}\Omega = \frac{1}{3}\int_{4\pi}[\tilde{I}(\mathbf{x},\mathbf{s},t) + 2\bar{I}^{+}(\mathbf{x},\mathbf{s},t) + 3I_{\mathrm{c}}(\mathbf{x},\mathbf{s},t)]\mathbf{s}\mathrm{d}\Omega. \quad (29)$$

From the above solution process, it can be seen that the present DUGKS is different in the flux reconstruction from the conventional FVM solver of RTE, in which the step scheme (first-order accurate) and the curved-line advection method (CLAM, second-order accurate) [43] are usually utilized. Compared to the fully implicit scheme, DUGKS calculations can be carried out in a local stencil, resulting in a much better parallel scalability. Moreover, the special treatments for temporal and spatial variables in DUGKS ensure a second-order accuracy in both time and space. It can be easily proved that the present DUGKS for a gray radiative transfer system is asymptotic preserving. The proof procedure is similar to those for phonon transport. A detailed analysis of the asymptotic property can be found in Ref. [37]. We only give a sketch of it in the Appendix.

IV. RESULTS AND DISCUSSION

Three test cases are presented to validate the numerical performance of the method in this section. The first addresses one-dimensional transient problems with collimated incident radiation. The rest are multidimensional radiative transfer problems in both homogenous and inhomogeneous media. All computations are performed on a machine with an Intel® Core™ i7-4790 CPU 3.6 GHz processor with 8.00 GB RAM and 64-bit operating system.

A. One-dimensional transient problems

The DUGKS now is applied to transient radiative transfer in a plane-parallel slab filled with an absorbing-scattering gray participating medium having two diffuse boundaries. One of the boundaries is subjected to a collimated beam. Owing to its wide application, this problem has been investigated by various methods, including FVM [10,44], MCM [23,26], and the integral equation (IE) method [45]. In this work, we consider three kinds of irradiation, namely, continuous collimated incidence, single square pulse collimated incidence, and truncated Gaussian pulse collimated incidence. The corresponding incident radiation can be written mathematically as follows:

$$I^{\mathrm{ext}}(\mathbf{x}_{\mathrm{w}},\mathbf{s},t) = I_0\delta(\mathbf{s}-\mathbf{s}_0), \quad t > 0,$$
$$I^{\mathrm{ext}}(\mathbf{x}_{\mathrm{w}},\mathbf{s},t) = I_0\delta(\mathbf{s}-\mathbf{s}_0), \quad 0 < t < t_{\mathrm{p}},$$

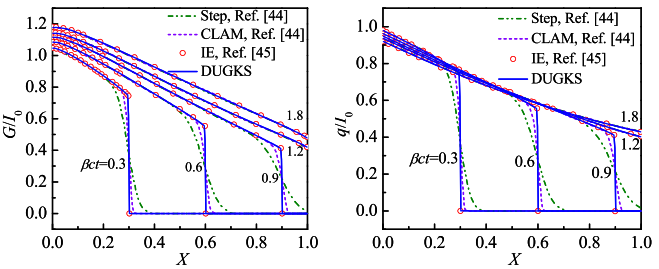

FIG. 1. Spatial and temporal distributions of radiation energy due to continuous collimated radiation: (a) incident radiation and (b) radiative flux.

$$I^{\mathrm{ext}}(\mathbf{x}_{\mathrm{w}},\mathbf{s},t) = I_0\delta(\mathbf{s}-\mathbf{s}_0)\exp\left[-4\ln 2\left(\frac{t-3t_{\mathrm{p}}}{t_{\mathrm{p}}}\right)^2\right], \quad 0 < t < 6t_{\mathrm{p}}, \quad (30)$$

where $\mathbf{s}_0$ is the irradiation direction, t_{p} is the incident pulse width, and I_0 is the maximum radiative intensity of the pulse. The irradiation is normal to the left face of the slab, namely, $\mathbf{s}_0 \cdot \mathbf{n}_{\mathrm{w}} = -1$. Initially, the medium inside the slab is cold and the medium emission is neglected ($I_{\mathrm{b}} = 0$) due to the ultrashort timescales of pulsed radiation. The extinction coefficient and the scattering albedo are homogeneous in the medium.

Figure 1 shows the incident radiation and radiation flux due to continuous collimated irradiation with $\beta = 1$ and $\omega = 0.5$. The DUGKS results are compared with solutions of the IE [45] and conventional FVM [44], in which an implicit scheme is employed for temporal discretization and a step scheme or CLAM scheme is employed for spatial discretization. In this case, the mesh and discrete angle set in DUGKS simulations are identical to those described in the literature [44]. Forty control angles and 300 uniform control volumes are used. It is seen from Fig. 1 that the DUGKS captures correctly the transient effect of light propagation due to the large speed of light compared to the local time and length scales, and produces accurate solutions as the IE has done. Due to the excessive numerical smearing, the step scheme and CLAM scheme cannot capture accurately the discontinuity in the incident radiation and radiation flux at the radiation wave front.

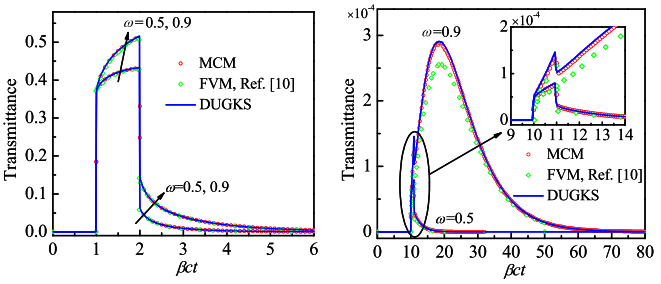

FIG. 2. Time history of transmittance due to square pulse irradiation with a width of $\beta c t_{\mathrm{p}} = 1$: (a) $\beta = 1$ and (b) $\beta = 10$.

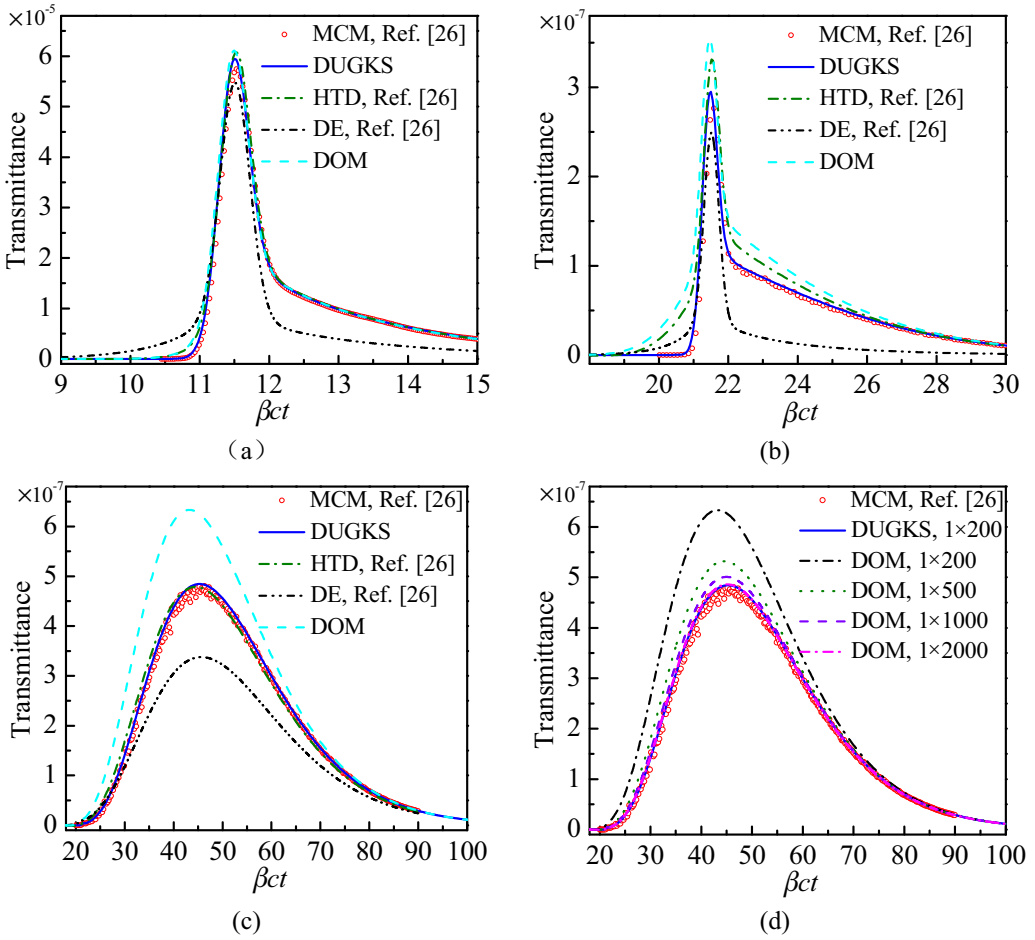

FIG. 3. Time history of transmittance due to Gauss pulse irradiation with a width of $\beta c t_p = 0.5$: (a) $\beta = 10, \omega = 0.5$; (b) $\beta = 20, \omega = 0.5$; (c) $\beta = 20, \omega = 0.9$; and (d) $\beta = 20, \omega = 0.9$.

Figure 2 displays the time-resolved transmittance due to square pulse irradiation with a width of $\beta c t_p = 1$. Transmittance is defined as the dimensionless net radiative heat flux at the exit boundary:

$$\text{Transmittance} = \frac{1}{\pi I_0} \int_{\mathbf{s}\cdot\mathbf{n}_w<0} (\mathbf{n}_w \cdot \mathbf{s}) I(\mathbf{x}_w, \mathbf{s}, t) \mathrm{d}\Omega. \quad (31)$$

Transmittance provides specific information about the media and is a significant measured signal in the analysis of transient radiative heat transfer. In DUGKS modeling, the grid number is uniform and the same for all cases considered, and the number of spatial grids is $N_x = 200$. The CFL number is fixed to 0.9. Forty equally spaced directions are taken for all cases, which may be of high computational cost in optically thick media but are not of concern for our present purpose. As seen from Fig. 2(b), the temporal distribution of transmittance has two local maxima for a big extinction coefficient of $\beta = 10\,\mathrm{m}^{-1}$ and scattering albedo ($\omega = 0.9$). The first peak occurs as soon as the direct pulse reaches the exit surface of the slab. The second peak is due to the scattered radiation and appears only in media where the scattering albedo is large. For comparison, the solutions obtained by conventional FVM [10] and MCM are also plotted in Fig. 2. The MCM solutions are taken as benchmarks. For $\beta = 1\,\mathrm{m}^{-1}$, the DUGKS, FVM, and MCM results are seen obviously to agree very well with each other. For $\beta = 10\,\mathrm{m}^{-1}$, the DUGKS solution has the same level of accuracy as the MCM, while the FVM underestimates the peak value of transmittance, especially for $\omega = 0.9$, even with a fine-grid system of $N_x = 500$. The reason for this is that photon transport is dominated by scattering in an optically thick regime. The error on the scattering term significantly reduces the accuracy of numerical simulations and needs careful handling.

To further demonstrate the numerical performance of DUGKS in an optically thick regime, the transient effects due to Gauss-shaped pulse irradiation with a width of $\beta c t_p = 0.5$ are also investigated by DOM, MCM, DUGKS, HTD, and DE, respectively. The spatial and angular discretization for DUGKS and DOM simulations is the same as that for the modeling of radiative transfer in the medium subject to a square pulse irradiation. The CFL number is set to 0.5. For DOM, the full explicit scheme is employed for temporal discretizing and the step scheme for spatial discretizing. Results obtained by these models are presented in Fig. 3. The numerical solutions of MCM are taken as benchmarks. Obviously, the results by DUGKS closely match the MCM solutions, no matter how large the optical thickness of the medium is. In an optically thick regime, DUGKS and the HTD model [26] have the same order of accuracy. Among these methods, the

TABLE I. Comparison of the computation times for DOM and DUGKS (RE indicates relative errors for the peak transmittance).

			$\beta = 1$		$\beta = 5$		$\beta = 10$		$\beta = 20$	
Method	Grid number	CFL number	CPU time (s)	RE (%)	CPU time (s)	RE (%)	CPU time (s)	RE (%)	CPU time (s)	RE (%)
DUGKS	200	0.5	10.28	0	2.14	0	1.03	0	0.51	0
		0.9	5.54	0.01	1.15	0.03	0.59	0.21	0.30	0.43
DOM	200	0.5	3.92	0.35	0.80	0.72	0.39	3.58	0.20	30.71
	500				4.34	0.51	2.29	0.63	1.23	9.82
	1000						8.35	0.37	4.48	3.42
	2000								16.80	0.33

DE model cannot predict the transmittance signal correctly. As for DOM, its numerical accuracy depends heavily on the density of spatial grids, and it requires a very fine grid system for predicting transient radiative transfer well in the medium having a big extinction coefficient, as shown in Fig. 3(d) and Table I. The computational time and relative errors at the peak point of transmittance curves of DOM and DUGKS for various extinction coefficients and $\omega = 0.9$ are compared and illustrated in Table I. The results by DUGKS with a CFL number of 0.5 are considered benchmarks for comparison here. It is found that the DUGKS requires a larger computational cost for all cases with the same grid number. The calculative inefficiency of DUGKS results from the flux reconstructions, where the absorbing and scattering effects are considered. Since DUGKS is more stable than the explicit DOM, the computational efficiency of DUGKS can be improved by using a coarse mesh or a larger CFL number; e.g., the CFL number is set to be 0.9. In fact, the satisfactory solutions can be obtained with a spatial grid number of 200, or even 100 by DUGKS, while a mesh refinement is required for DOM simulations in optically thick medium to reduce the calculation error, as shown in Fig. 3(d) and Table I. In order to obtain the convergent solutions having approximately the same accuracy as DUGKS, grid numbers of 1000 and 2000 are required in DOM for $\beta = 10$ and $\beta = 20\,\mathrm{m}^{-1}$, respectively, as shown in Table I. Table I also reveals that the mesh refinement in DOM increases the CPU times considerably. In this case, DUGKS has great computational advantage over the explicit DOM.

B. Two-dimensional steady-state problems

The second test case considers the steady-state radiative heat transfer in the two-dimensional (2D) square gray participating media with the side length of L enclosed by four boundaries. All boundaries of the enclosure are diffusive and gray. This problem has been widely used in the literature [13,46,47] and is the representative 2D benchmark problem for validating numerical method to solve the RTE. In the present work, this steady problem is modeling as a transient problem by DUGKS, and a steady-state solution is achieved when the relative difference of the incident radiation between two successive 100 time steps is less than 10^{-6}. Both radiative equilibrium and radiative nonequilibrium are considered in this work. Since there is no irradiation, we have

$$I_c(\mathbf{x},\mathbf{s},t) \equiv 0, \quad I(\mathbf{x},\mathbf{s},t) = I_d(\mathbf{x},\mathbf{s},t). \tag{32}$$

For the DUGKS modeling, a uniform mesh system in Cartesian coordinates is used for physical space and the Gauss-Legendre quadrature is utilized for angular discretization. The direction cosine of zenith angle μ is discretized into N_μ points in $[-1, 1]$. The azimuth angle φ is discrete into N_φ points in $[0, \pi]$ ($[0, 2\pi]$ for three-dimensional cases). The CFL number is taken to be 0.5 unless stated otherwise.

The radiative equilibrium problem is considered first. In this case, the bottom boundary of the enclosure is kept hot and has unity emissive power, whereas the other three boundaries are kept cold with a dimensionless temperature of 0 K. The medium is homogeneous with a constant scattering albedo $\omega = 1$. When radiative equilibrium is reached, the incident radiation is balanced with the blackbody emission from the medium at every location. For comparison, this problem is investigated by the present DUGKS and a published FVM code (developed by Chai, called RAT) [48,49]. If $\tau = \beta L < 2$, the angular discretization in both DUGKS and FVM simulations is set to be $N_\mu \times N_\varphi = 16 \times 16$. For a higher value of the extinction coefficient, $\tau \geqslant 2$, a smaller number of discrete directions is used, that is, $N_\mu \times N_\varphi = 8 \times 16$. Figure 4(a) and 4(b) display the net radiative flux at the hot wall obtained by these two methods with different mesh resolutions. It is found that DUGKS is insensitive to grid refinement for a fixed angular discretization. This indicates that a coarse grid system (e.g., $N_x \times N_y = 40 \times 40$) is sufficient to obtain convergent solutions. However, in FVM simulations, a fine mesh system is required to obtain grid-independent results for a higher value of the optical thickness (e.g., $\tau = 5, 10, 20$). For all optical thicknesses considered, the DUGKS solutions are in a good agreement with the convergence outcomes by FVM. The total CPU time of the DUGKS and the FVM simulations is compared in Table II. It is observed from Table II that the DUGKS takes more computational time for all optical thicknesses with the same mesh system of 40×40. The reason for this is that DUGKS solves a steady-state problem as a limiting case of a transient problem, which results in computational inefficiency. However, the FVM converges very slowly in the optically thick regime and takes much more time for the convergence results because of the use of much denser mesh. In this case, the FVM requires grid numbers of at least 200×200 and 400×400 for obtaining the convergent solutions for $\tau = 10$ and 20, respectively, while the DUGKS requires only 40×40 grids, independent of optical thickness. This revealed that the present DUGKS is a promising approach with high efficiency and satisfactory accuracy for simulating radiative heat transfer in an optically thick medium,

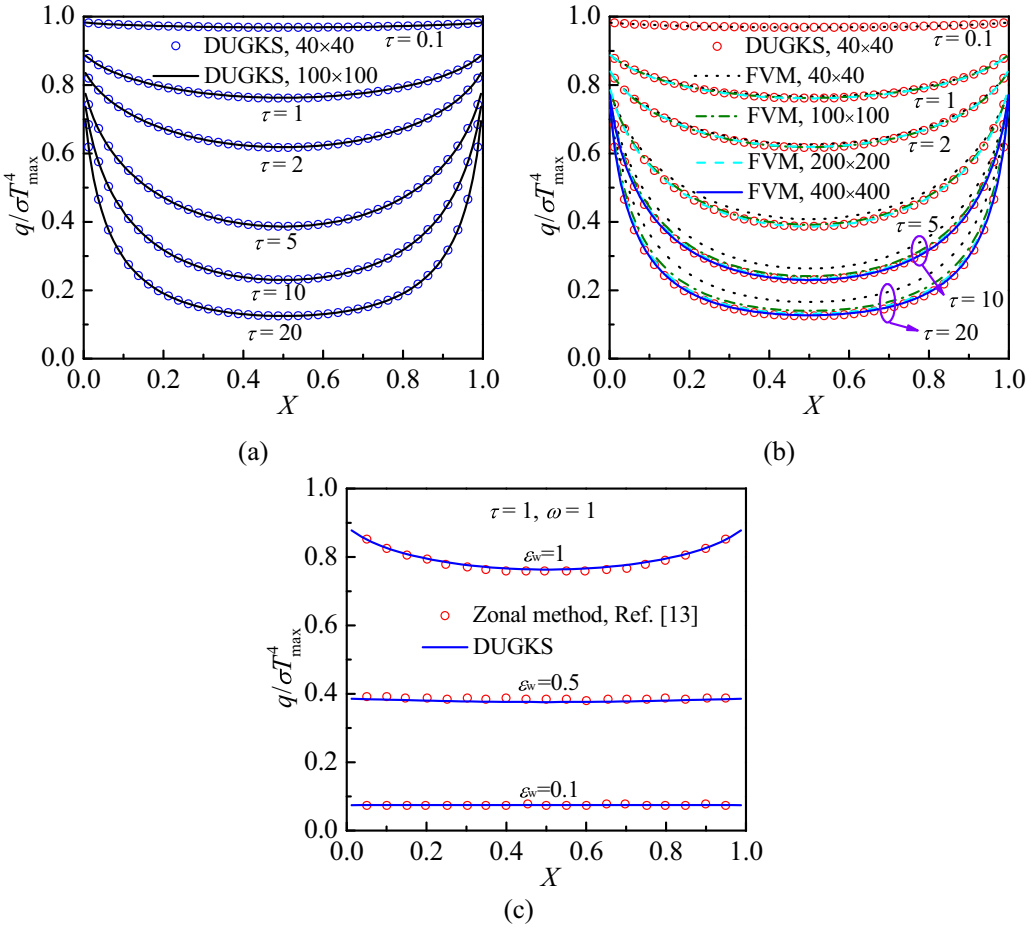

FIG. 4. Nondimensional net radiative heat flux at the hot wall for the radiative equilibrium problem: (a) DUGKS solutions at different optical thickness, (b) FVM solutions at different optical thickness, and (c) the effects of wall emissivity.

and its computational efficiency advantage over the FVM will become increasingly evident as the optical thickness is further increased.

The effects of wall emissivity in the case of $\tau = 1$ are investigated by the present DUGKS and displayed in Fig. 4(c). After the grid independence and ray independence tests, a 40×40 uniform grid system and an 8×16 discrete angle set are employed in the DUGSK simulations. In Fig. 4(c), the variations of dimensionless net radiative flux at the hot boundary are shown for wall emissivities $\varepsilon_w = 0.1, 0.5$, and 1, respectively. The DUGKS solutions are found to compare very well with the results by the zonal method [13].

The radiative nonequilibrium problem is also investigated here. In this case, all four boundaries of the enclosure are cold and the medium is kept hot with a unitary emission ($I_b = 1/\pi$). After the independence test, the same mesh system $N_x = N_y = 40$ is employed for all cases and the discrete angles $N_\mu \times N_\varphi = 8 \times 8, 8 \times 8$, and 4×8 are employed for $\tau = 0.1, 1$, and 10, respectively. Figures 5(a) and 5(b) shows the variation of net heat flux on the bottom wall with different scattering albedos and optical thicknesses. It is seen from Fig. 5 that the results obtained by DUGKS agree well with those by the collapsed dimension method (CDM) [47] and the zonal method [13]. As shown in Fig. 5(b), there are some small deviations between the

TABLE II. Comparison of the CPU times of the DUGKS and the FVM in the modeling of radiative equilibrium problem.

		CPU time (s)					
Methods	Mesh ($N_x \times N_y$)	$\tau = 0.1$	$\tau = 1$	$\tau = 2$	$\tau = 5$	$\tau = 10$	$\tau = 20$
DUGKS	40×40	3.65	2.71	2.95	4.23	6.474	10.58
	40×40	0.17	0.11	0.19	0.53	1.20	2.82
FVM	100×100		1.05	1.44	3.81	9.28	24.51
	200×200				16.05	41.23	140.06
	400×400					204.02	625.21

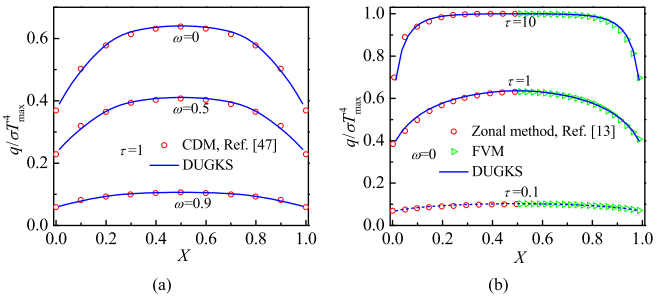

FIG. 5. Nondimensional net wall radiative heat flux at the radiative nonequilibrium: (a) effects of scattering albedo and (b) effects of extinction coefficient.

two calculation models, particularly near the boundary with a sharp gradient of radiation intensity as the optical thickness of the medium increases. Nevertheless, the maximum deviation is less than 1.8%. For further comparison, the results calculated by the FVM code RAT [48,49] are also plotted in Fig. 5(b). It is found that DUGKS leads to considerably accurate outcomes like the FVM.

To test the numerical stability of DUGKS, a special case, radiative transfer in a unit square enclosure within an absorbing-emitting medium having a Gaussian emissive field is studied. This case can be considered a special kind of radiative nonequilibrium problem with the nonhomogenous emission

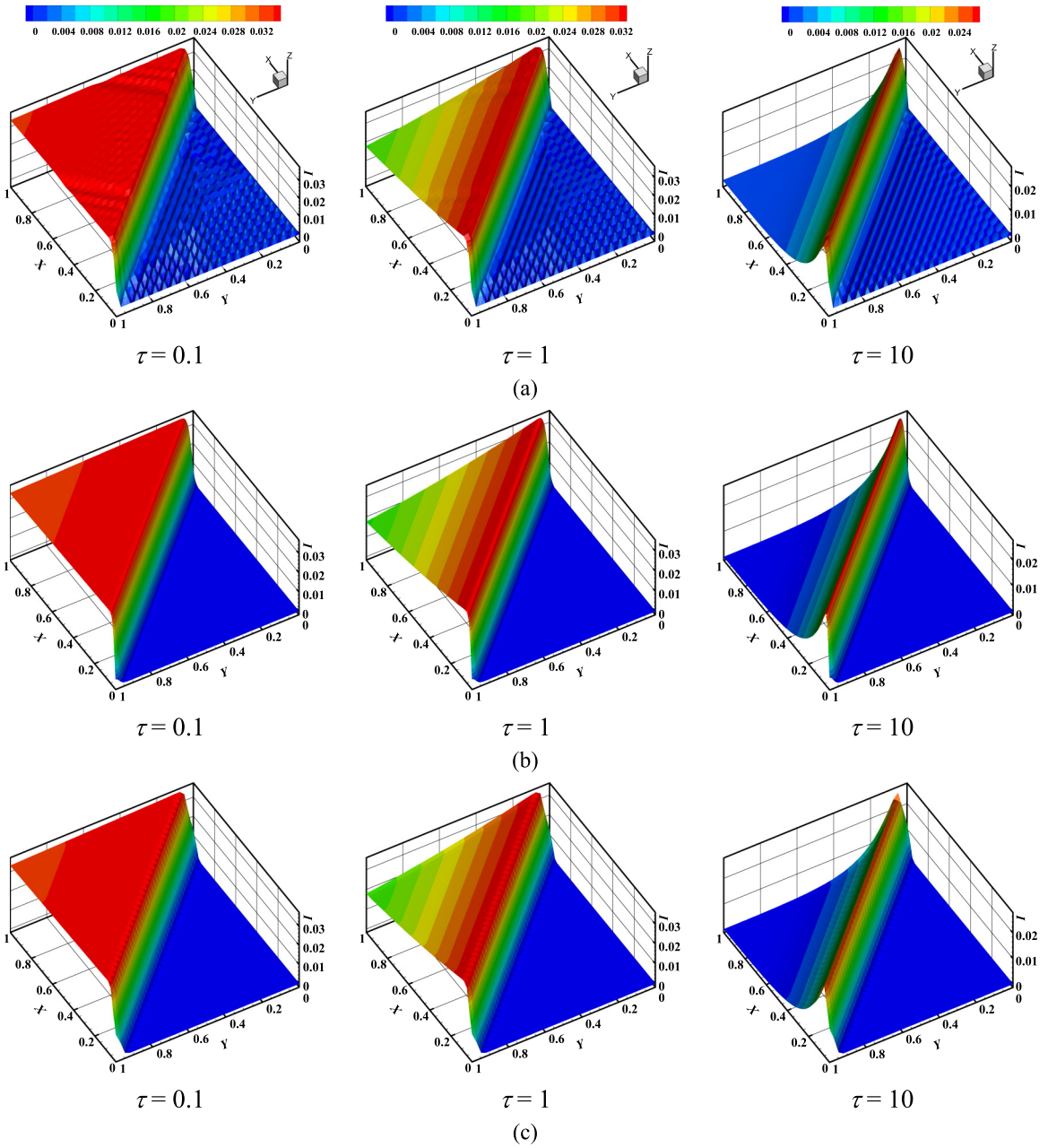

FIG. 6. Radiative intensity distributions in the square enclosure with different optical thicknesses: (a) Galerkin FEM solutions, (b) analytical solutions, and (c) DUGKS solutions.

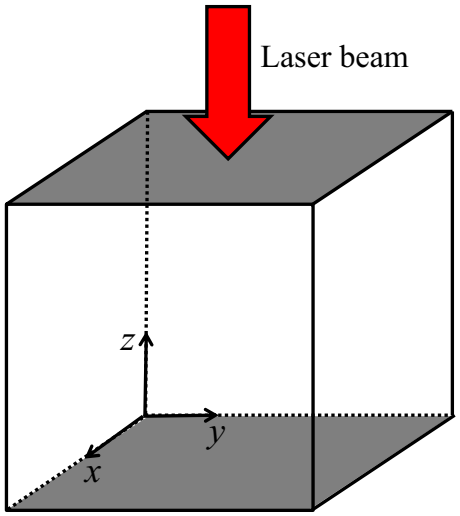

FIG. 7. Schematic of the cubic enclosure subjected to an incident short-pulse laser.

power

$$I_b(x,y) = \frac{1}{\beta}\exp\left[-\frac{1}{\alpha^2}\left(\frac{x+y}{\sqrt{2}} - c\right)^2\right], \quad (33)$$

in which the emission profile parameters are selected as $\alpha = 0.02$ and $c = \sqrt{2}/2$. The boundary condition is prescribed on the inflow boundaries with null emission. Considering the incident direction $\mathbf{s} = (\sqrt{2}/2, \sqrt{2}/2)$, the analytical solution to this problem can be obtained in Refs. [18,46]. DUGKS is applied to solve the intensity distribution in the medium for different values of $\tau = 0.1, 1$, and 10. The spatial grid system in DUGKS simulations is the same as that for the radiative equilibrium case. The corresponding results are compared to numerical results obtained by the Galerkin FEM with the same meshes and analytical solutions and displayed in Fig. 6. As seen from Fig. 6, DUGKS is almost stable with slightly spurious oscillations for all optical thicknesses while the Galerkin FEM produces an apparent oscillating intensity field, especially at small optical thickness. These nonphysical oscillations result from the inappropriate spatial discretization for a strong convection-dominated equation, and special stabilization techniques (e.g., upwind scheme and least-squares scheme) [50–52] are usually required to remove such oscillations.

C. Three-dimensional multiscale problem

In this section we present an application of the proposed DUGKS to a three-dimensional multiscale radiative transfer problem. As illustrated in Fig. 7, a unit cube is filled with a nonhomogenous absorbing-scattering medium. The right-handed coordinate system is created with the coordinate origin located at one of the vertices. The extinction coefficient of the medium varies vertically and is governed by the following expression:

$$\beta = \beta_{\max} - 2(\beta_{\max} - \beta_{\min})|z - 0.5|, \quad 0 \leqslant z \leqslant 1, \quad (34)$$

in which $\beta_{\max}$ and $\beta_{\min}$ are the maximum and minimum values of extinction coefficient, respectively. Equation (34) indicates that the extinction coefficient distributes symmetrically, increases linearly with z for $z < 0.5$, and reaches the peak value $\beta_{\max}$ at $z = 0.5$, then decreases with z. The minimum extinction coefficient $\beta_{\min}$ occurs at the face $z = 0$ or $z = 1$. Additionally, the scattering albedo ω is assumed to be constant in this work. At $t = 0$, the top face of the cubic enclosure is irradiated by an incident short-pulse laser, and the direction of the collimated irradiation is normal to the top face. The intensity of the laser pulse is given by

$$I(x,y,z=1,\mathbf{s}_0,t) = I_0\delta(\mathbf{s}-\mathbf{s}_0), \quad 0 < t < t_p, \quad (35)$$

where I_0 is the radiative intensity of the square pulse, $\mathbf{s}_0$ is the irradiation direction, and $t_p = 1/(\beta_{\max}c)$ is the width of the square pulse. According to Eq. (35), the medium is free from irradiation after t_p. The media are supposed to be nonrefracting and photons travel with the same velocity. All boundaries are cold and nonreflecting.

This transient radiative transfer problem associated with the spatially varying radiative property is of great interest due to its frequent occurrence in both nature (e.g., multilevel cloud systems, biological tissues, etc.) and technological applications. For this problem, no analytical solution is available and MCM is difficult and very time consuming. A wide spatial range of optical thickness divides the computational domain into the diffusive regime and kinetic regime, and therefore brings great challenges for numerical simulations. We employ DUGKS to solve this problem with three different uniform meshes, namely, $20 \times 20 \times 50$, $20 \times 20 \times 100$, and $20 \times 20 \times 200$. Here a finer grid in the streamwise direction is used to accurately capture the variance of optical thickness. Additionally, the angular discretization $N_\mu \times N_\varphi = 16 \times 32$ is utilized here to reduce the ray effect as much as possible. For different mesh resolutions, we fixed the time step $c\Delta t = 0.0125$ to reduce the effect of time step on numerical solutions. In addition, we fixed the extinction coefficient $\beta_{\min} = 1$ to form a kinetic regime. The effects of the maximum value and scattering albedo are investigated.

Figure 8 shows the dimensionless transmittance signals, which are defined as

$$T(t) = \frac{1}{I_0}\int_0^1\int_0^1\int_{\mathbf{s}\cdot\mathbf{n}_w<0}(\mathbf{n}_w\cdot\mathbf{s})I(x,y,z=0,\mathbf{s},t)\mathrm{d}\Omega\mathrm{d}x\mathrm{d}y. \quad (36)$$

Figures 8(a) and 8(b) display the predicted transmittance signals at a smaller $\beta_{\max} = 20$ while Figs. 8(c) and 8(d) display the transmittance signals at a lager $\beta_{\max} = 50$. In general, the temporal transmittance exhibits a sharp peak. The transmittance stay zero until photons travel across the medium and reach the boundary $z = 0$. Then the transmittance increases significantly up to the peak value due to the scattering within the medium. Since the medium in the middle layer has a larger optical thickness, it takes a long time for scattered photons to reach the right boundary due to the frequent scatter event in the diffusive regime. It can be also seen from Fig. 8 that larger value of at $\beta_{\max}$ results in a smaller peak value of transmittance signals and larger peak time. With the increase of scattering

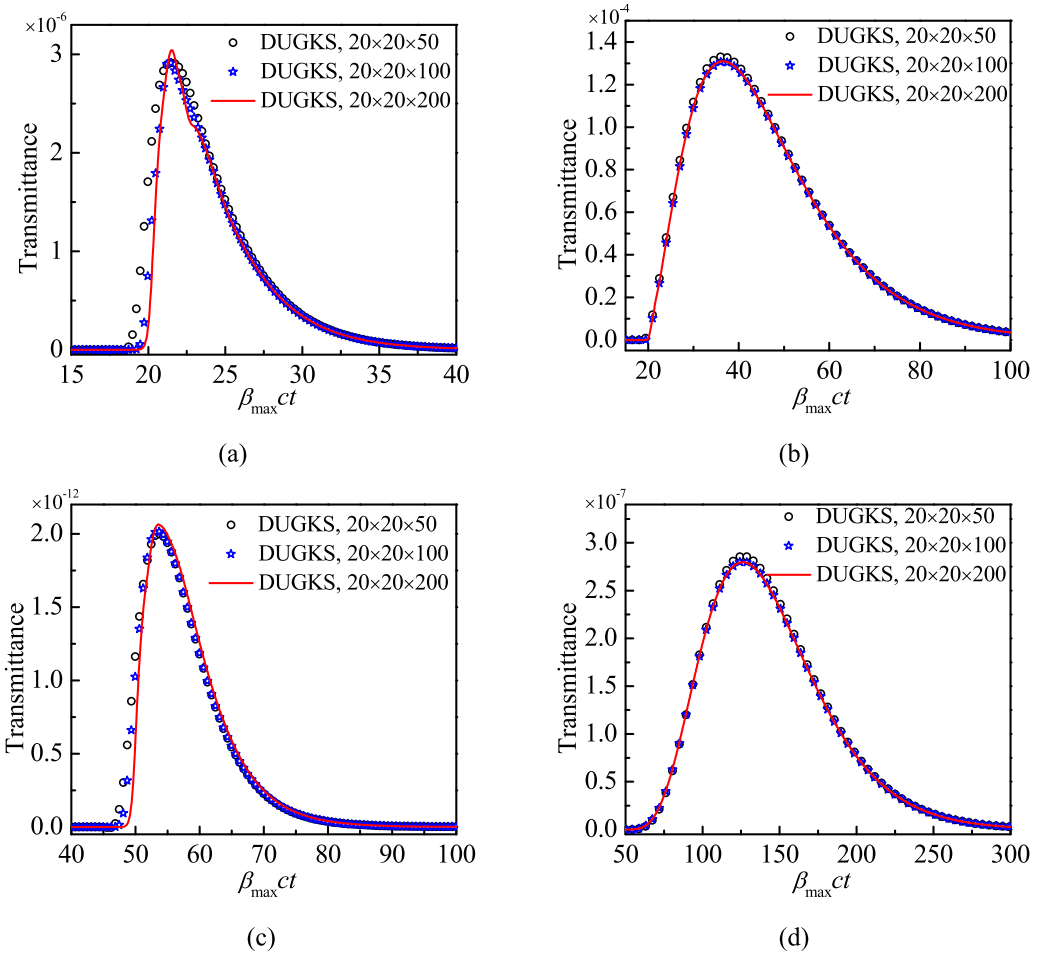

FIG. 8. The predicted transient transmittance signals for various parameters: (a) $\beta_{\max} = 20$, $\omega = 0.5$; (b) $\beta_{\max} = 20$, $\omega = 0.95$; (c) $\beta_{\max} = 50$, $\omega = 0.5$; and (d) $\beta_{\max} = 50$, $\omega = 0.95$.

albedo, the diffuse component becomes dominant and the transmittance increases by orders of magnitude. Comparing results by different mesh resolutions, the DUGKS solutions exhibit low grid dependence especially for large scattering albedo. This suggests that DUGKS is flexible enough to deal with the diffusive and the kinetic regimes and offers a robust tool for multiscale radiative transfer problem where both regimes can be found.

V. CONCLUSION

Radiative transfer in participating media has multiscale characteristics due to the influence of optical thickness (the reciprocal of the Knudsen number). If the optical thickness is much smaller than unity, photons fall in the ballistic regime where the ballistic transport is dominated. If the optical thickness is much larger than unity, photons fall in the diffusive regime where the radiative transfer by diffusion is dominated. All conventional methods based on the RTE such as MCM, DOM, FVM, and so on converge slowly when the solution domain is close to the diffusive regime. Accordingly, the computational requirements increase linearly with the dth (d denotes the dimensionality of the solution domain) power of the optical thickness.

In this work, we presented an asymptotic-preserving discrete unified gas kinetic scheme for efficiently and accurately solving the transient radiative transfer equation in the whole range of optical thicknesses. In the numerical scheme, the discrete ordinate method is applied to discretize angle direction, the finite volume method is used for the spatial discretization, and a semi-implicit scheme is adopted for the time integration.

In contrast with the conventional finite volume method, the flux at the cell interface in the DUGKS is approximated by integrating the RTE along the characteristic line, respecting the physics of radiative transport like the MCM. As a result, the spurious diffusion is effectively mitigated. In the DUGKS, each time step can be computed explicitly and cheaply without subiteration and the CFL restriction on the time step size is removed. Our developed scheme does preserve the asymptotic diffusion limit of the radiative transfer system without resolving the mesh size, and is correct, efficient, and stable to solve the radiative transfer equation in the optically thin, optically thick, and transition regimes.

For validation purposes, the present method is tested by a set of radiative transport problems including one-dimensional transient radiative transfer and multidimensional steady radiative transfer. The numerical results obtained by the present method have been compared with other different numerical schemes. These comparisons reveal that the proposed DUGKS

has a good performance in both transient and steady modeling. Since the spurious diffusion is effectively mitigated, the present method does improve significantly the accuracy in optically thick media avoiding using a fine computational grid system compared to the conventional methods like DOM and FVM. Moreover, the present method is found to be much more efficient than the conventional numerical methods when the physical conditions are close to the radiative diffusion regime. The computational results also confirm the promising and excellent capability of the present method in capturing the sharp spatial discontinuities in the radiation field and modeling multiscale radiative transfer.

The present work is currently limited to the regular geometries and isotropic scattering. In future work, we will extend the DUGKS to radiative transfer in complex configurations based on the unstructured mesh technique. We will also modify the DUGKS for solving the radiative transfer in anisotropic scattering media. In addition, we can extend the DUGKS to frequency-dependent radiative transfer and polarized radiative transfer.

ACKNOWLEDGMENTS

This work has been supported by the National Natural Science Foundation of China (Grants No. 51422602 and No. 51706053).

APPENDIX

The asymptotic property of DUGKS is analyzed here. More precisely, we show that the present DUGKS is able to give a suitable numerical approximation in the limit of both β large and small. Let us first consider the asymptotic behavior of the scheme in the limit where β tends to infinity. For simplicity, the external irradiation is ignored. Thus all terms involving the component $I_c(\mathbf{x},\mathbf{s},t)$ can be omitted. Since we are mainly interested in optically thick limits leading to diffusion equations, we apply the following change of variables,

$$t \to \varepsilon^2 t_0, \quad \mathbf{x} \to \varepsilon \mathbf{x}_0, \tag{A1}$$

where ε is small parameter related to the MFP of photons. Inserting Eq. (A1) into Eq. (4), Eq. (4) can be rewritten as

$$\frac{\varepsilon^2}{c}\frac{\partial I}{\partial t_0} + \varepsilon \mathbf{s}\cdot\frac{\partial I}{\partial \mathbf{x}_0} = -\beta I + \beta(1-\omega)I_b + \frac{\beta\omega}{4\pi}\int_{4\pi} I\,\Phi \mathrm{d}\Omega'. \tag{A2}$$

In order to analyze multiscale effects of the underlying equations, it is often advisable to apply a formal asymptotic analysis and express all variables in the form of the Hilbert expansion in the parameter ε by

$$I = I^{(0)} + \varepsilon I^{(1)} + \cdots. \tag{A3}$$

We substitute this expansion into Eq. (A2) and compare the equal-order terms in ε,

$$\varepsilon^0 : -\beta I^{(0)} + \beta(1-\omega)I_b + \frac{\beta\omega}{4\pi}\int_{4\pi} I^{(0)}\mathrm{d}\Omega' = 0, \tag{A4}$$

$$\varepsilon : \mathbf{s}\cdot\frac{\partial I^{(0)}}{\partial \mathbf{x}_0} = -\beta I^{(1)} + \frac{\beta\omega}{4\pi}\int_{4\pi} I^{(1)}\mathrm{d}\Omega'. \tag{A5}$$

Integrating Eq. (A4) over the solid angle yields

$$\int_{4\pi} I^{(0)}\mathrm{d}\Omega' = 4\pi I_b, \quad I^{(0)} = I_b. \tag{A6}$$

Noticing that $I^{(0)}$ is angle independent and integrating Eq. (A5) over the solid angle yields

$$I^{(1)} = \frac{1}{\beta}\mathbf{s}\cdot\frac{\partial I_b}{\partial \mathbf{x}_0}. \tag{A7}$$

Substituting Eqs. (A6) and (A7) into Eq. (A3), the radiative intensity can be approximated as

$$\begin{aligned} I &= I_b - \frac{\varepsilon}{\beta}\mathbf{s}\cdot\frac{\partial I_b}{\partial \mathbf{x}_0} + O(\varepsilon^2) \approx I_b - \frac{\varepsilon}{\beta}\mathbf{s}\cdot\frac{\partial I}{\partial \mathbf{x}_0} + O(\varepsilon^2) \\ &\approx I_b - \frac{1}{\beta}\mathbf{s}\cdot\frac{\partial I}{\partial \mathbf{x}} + O(\varepsilon^2). \end{aligned} \tag{A8}$$

The above expression is also called the Rosseland approximation in radiation theory. Similarly, integrating Eq. (4) over the solid angle and combining with Eqs. (A6) and (A8), the macroscopic diffusion equation for radiative transport can be obtained [26],

$$\frac{1}{c}\frac{\partial G}{\partial t} + \frac{\partial}{\partial \mathbf{x}}\cdot\left(\frac{1}{3\beta}\frac{\partial G}{\partial \mathbf{x}}\right) = \beta(1-\omega)(4\pi I_b - G), \tag{A9}$$

where we have made use of the property of angular quadrature,

$$\sum_k \mathbf{s}_k w_k = 0, \quad \sum_k \mathbf{s}_k \mathbf{s}_k w_k = \frac{4\pi}{3}\delta_{ij}. \tag{A10}$$

For the DUGKS formula, plugging Eq. (A8) into Eq. (16) and integrating Eq. (15) over the solid angle yields that

$$\begin{aligned} &\frac{G(\mathbf{x}_j,t_{n+1}) - G(\mathbf{x}_j,t_n)}{c\Delta t} - \sum_f \frac{\Delta S_f}{3\beta V_j}\mathbf{n}_f\cdot\nabla G(\mathbf{x}_f,t_{n+1/2}) \\ &= \frac{\beta}{2}(1-\omega)[4\pi I_b(\mathbf{x}_j,t_{n+1}) - G(\mathbf{x}_j,t_{n+1}) \\ &\quad + 4\pi I_b(\mathbf{x}_j,t_n) - G(\mathbf{x}_j,t_n)], \end{aligned} \tag{A11}$$

which is a consistent approximation of Eq. (A9). This indicates that the DUGKS is AP in the thick diffusive limit.

Now we discuss the AP property of the DUGKS in the optically thin limit. Noticing that $\beta c\Delta t \ll 1$ in this case, Eqs. (20) and (12) reduce to

$$I(\mathbf{x}_f,\mathbf{s}_k,t_{n+1/2}) = I(\mathbf{x}_j - \mathbf{s}_k ch, \mathbf{s}_k, t_n), \tag{A12}$$

$$\begin{aligned} &\frac{1}{c}\frac{I(\mathbf{x}_j,\mathbf{s}_k,t_{n+1}) - I(\mathbf{x}_j,\mathbf{s}_k,t_n)}{\Delta t} \\ &+ \frac{1}{V_j}\sum_f (\mathbf{s}_k\cdot\mathbf{n}_f) I(\mathbf{x}_f,\mathbf{s}_k,t_{n+1/2})\Delta S_f = 0, \end{aligned} \tag{A13}$$

which is a consistent discretization of RTE in the optically thin limit where the convection is dominant for photon transport. In other word, DUGKS is also AP in optically thin regions.

[1] M. Malinauskas, A. Zcaronukauskas, S. Hasegawa, Y. Hayasaki, V. Mizeikis, R. Buividas, C. Caronardas, and S. Juodkazis, Light: Sci. Appl. **5**, e16133 (2016).

[2] S. R. Arridge, Inverse Probl. **15**, R41 (1999).

[3] F. Wang, L. Ma, Z. Cheng, J. Tan, X. Huang, and L. Liu, Renewable Sustainable Energy Rev. **73**, 935 (2017).

[4] F. C. Lockwood and N. G. Shah, Symp. Combust. **18**, 1405 (1981).

[5] K. J. Grant, J. A. Piper, D. J. Ramsay, and K. L. Williams, Appl. Opt. **32**, 416 (1993).

[6] P. Rairoux *et al.*., Appl. Phys. B **71**, 573 (2000).

[7] M. H. N. Naraghi, B. Litkouhi, and B. T. F. Chung, J. Heat Transfer **110**, 456 (1988).

[8] K. F. Evans, J. Atmos. Sci. **55**, 429 (1998).

[9] P. Rath, S. C. Mishra, P. Mahanta, U. K. Saha, and K. Mitra, Numer. Heat Transfer Part A **44**, 183 (2003).

[10] S. C. Mishra, P. Chugh, P. Kumar, and K. Mitra, Int. J. Heat Mass Transfer **49**, 1820 (2006).

[11] W. A. Fiveland, J. Heat Transfer **106**, 699 (1984).

[12] G. D. Raithby and E. H. Chui, J. Heat Transfer **112**, 415 (1990).

[13] W. A. Fiveland and J. P. Jessee, J. Thermophys. Heat Transfer **8**, 426 (1994).

[14] J. M. Zhao and L. H. Liu, Numer. Heat Transfer Part B **50**, 473 (2006).

[15] Y. Zhang, H. L. Yi, and H. P. Tan, Int. J. Heat Mass Transfer **56**, 411 (2013).

[16] J. Sun, K. Luo, H. L. Yi, and H. P. Tan, J. Quant. Spectrosc. Radiat. Transfer **164**, 54 (2015).

[17] K. Luo, Z. H. Cao, H. L. Yi, and H. P. Tan, J. Quant. Spectrosc. Radiat. Transfer **135**, 66 (2014).

[18] J. M. Zhao, J. Y. Tan, and L. H. Liu, J. Comput. Phys. **232**, 431 (2013).

[19] H. L. Yi, C. H. Wang, and H. P. Tan, Int. J. Heat Mass Transfer **79**, 437 (2014).

[20] B. C. Wilson and G. Adam, Med. Phys. **10**, 824 (1983).

[21] F. A. Kulacki, *Handbook of Thermal Science and Engineering* (Springer, Berlin, 2017).

[22] P. J. Coelho, J. Quant. Spectrosc. Radiat. Transfer **145**, 121 (2014).

[23] M. Roger and N. Crouseilles, J. Quant. Spectrosc. Radiat. Transfer **116**, 110 (2013).

[24] M. Lemou and L. Mieussens, SIAM J. Sci. Comput. **31**, 334 (2010).

[25] P. J. Coelho, N. Crouseilles, P. Pereira, and M. Roger, J. Quant. Spectrosc. Radiat. Transfer **172**, 36 (2016).

[26] M. Roger, C. Caliot, N. Crouseilles, and P. Coelho, J. Comput. Phys. **275**, 346 (2014).

[27] L. Mieussens, J. Comput. Phys. **253**, 138 (2013).

[28] W. Sun, S. Jiang, and K. Xu, J. Comput. Phys. **285**, 265 (2015).

[29] W. Sun, S. Jiang, K. Xu, and S. Li, J. Comput. Phys. **302**, 222 (2015).

[30] W. Sun, S. Jiang, and K. Xu, Commun. Comput. Phys. **22**, 889 (2017).

[31] W. Sun, S. Jiang, and K. Xu, J. Comput. Phys. **351** (2017).

[32] Z. Guo, K. Xu, and R. Wang, Phys. Rev. E **88**, 033305 (2013).

[33] Z. Guo, R. Wang, and K. Xu, Phys. Rev. E **91**, 033313 (2015).

[34] R. Wang, Ph.D. thesis, Hong Kong University of Science and Technology, 2015.

[35] L. Zhu and Z. Guo, Phys. Rev. E **95**, 023113 (2017).

[36] P. Wang, Y. Zhang, and Z. Guo, Int. J. Heat Mass Transfer **113**, 217 (2017).

[37] Z. Guo and K. Xu, Int. J. Heat Mass Transfer **102**, 944 (2016).

[38] X. P. Luo and H. L. Yi, Int. J. Heat Mass Transfer **114**, 970 (2017).

[39] J. R. Howell, R. Siegel, and M. P. Mengüç, *Thermal Radiation Heat Transfer,* 5th ed. (Hemisphere, New York, 2010).

[40] M. F. Modest, *Radiative Heat Transfer,* 2nd ed. (Academic Press, New York, 2003).

[41] P. J. Coelho, J. Quant. Spectrosc. Radiat. Transfer **73**, 231 (2002).

[42] M. A. Ramankutty and A. L. Crosbie, J. Quant. Spectrosc. Radiat. Transfer **57**, 107 (1997).

[43] B. V. Leer, J. Comput. Phys. **14**, 361 (1974).

[44] J. C. Chai, Numer. Heat Transfer Part B **44**, 187 (2003).

[45] Z.-M. Tan and P.-F. Hsu, J. Heat Transfer **123**, 466 (2001).

[46] H. L. Yi, F. J. Yao, and H. P. Tan, Phys. Rev. E **94**, 023312 (2016).

[47] S. C. Mishra, P. Talukdar, D. Trimis, and F. Durst, Int. J. Heat Mass Transfer **46**, 3083 (2003).

[48] J. C. Chai, H. O. S. Lee, and S. V. Patankar, Numer. Heat Transfer Part B **26**, 225 (1994).

[49] J. C. Chai, H. O. S. Lee, and S. V. Patankar, J. Thermophys. Heat Transfer **8**, 419 (2012).

[50] S. Richling, E. Meinköhn, N. Kryzhevoi, and G. Kanschat, Astron. Astrophys. **380**, 776 (2001).

[51] J. P. Pontaza and J. N. Reddy, J. Quant. Spectrosc. Radiat. Transfer **95**, 387 (2005).

[52] L. Zhang, J. M. Zhao, and L. H. Liu, J. Heat Transfer **138**, 064502 (2016).